

J. L. Griffin, D. Muller, R. Woograsingh, V. Jowatt, A. Hindmarsh, J. K. Nicholson and J. E. Martin

Physiol Genomics 11:195-203, 2002. First published Oct 15, 2002;
doi:10.1152/physiolgenomics.00100.2002

You might find this additional information useful...

This article cites 31 articles, 6 of which you can access free at:

<http://physiolgenomics.physiology.org/cgi/content/full/11/3/195#BIBL>

This article has been cited by 3 other HighWire hosted articles:

High Resolution 1H NMR-based Metabolomics Indicates a Neurotransmitter Cycling Deficit in Cerebral Tissue from a Mouse Model of Batten Disease

M. R. Pears, J. D. Cooper, H. M. Mitchison, R. J. Mortishire-Smith, D. A. Pearce and J. L. Griffin

J. Biol. Chem., December 30, 2005; 280 (52): 42508-42514.

[\[Abstract\]](#) [\[Full Text\]](#) [\[PDF\]](#)

Defining a metabolic phenotype in the brain of a transgenic mouse model of spinocerebellar ataxia 3

J. L. Griffin, C. K. Cemal and M. A. Pook

Physiol Genomics, February 13, 2004; 16 (3): 334-340.

[\[Abstract\]](#) [\[Full Text\]](#) [\[PDF\]](#)

Charting the effects of antioxidant therapy in the diseased brain: Focus on "Vitamin E deficiency and metabolic deficits in neuronal ceroid lipofuscinosis described by bioinformatics"

I. Jarvela and S. B. Glueck

Physiol Genomics, December 3, 2002; 11 (3): 183-184.

[\[Full Text\]](#) [\[PDF\]](#)

Updated information and services including high-resolution figures, can be found at:

<http://physiolgenomics.physiology.org/cgi/content/full/11/3/195>

Additional material and information about *Physiological Genomics* can be found at:

<http://www.the-aps.org/publications/pg>

This information is current as of July 5, 2009 .

Vitamin E deficiency and metabolic deficits in neuronal ceroid lipofuscinosis described by bioinformatics

J. L. GRIFFIN,¹ D. MULLER,³ R. WOGRASINGH,¹ V. JOWATT,²
A. HINDMARSH,² J. K. NICHOLSON,¹ AND J. E. MARTIN²

¹Biological Chemistry, Biomedical Sciences, Faculty of Medicine, Imperial College of Science, Technology and Medicine, London SW7 2AZ; ²Histopathology, Barts and the London, Queen Mary's School of Medicine and Dentistry, The Royal London Hospital, Whitechapel, London E1 1BB; and ³Institute of Child Health, London WC1 N1EH, United Kingdom

Submitted 6 August 2002; accepted in final form 30 September 2002

Griffin, J. L., D. Muller, R. Woograsingh, V. Jowatt, A. Hindmarsh, J. K. Nicholson, and J. E. Martin. Vitamin E deficiency and metabolic deficits in neuronal ceroid lipofuscinosis described by bioinformatics. *Physiol Genomics* 11: 195–203, 2002. First published October 15, 2002; 10.1152/physiolgenomics.00100.2002.—The *mnd* mouse, a model of neuronal ceroid lipofuscinosis (NCL), has a profound vitamin E deficiency in sera and brain, associated with cerebral deterioration characteristic of NCL. In this study, the vitamin E deficiency is corrected using dietary supplementation. However, the histopathological features associated with NCL remained. With use of a bioinformatics approach based on high-resolution solid and solution state ¹H-NMR spectroscopy and principal component analysis (PCA), the deficits associated with NCL are defined in terms of a metabolic phenotype. Although vitamin E supplementation reversed some of the metabolic abnormalities, in particular the concentration of phenylalanine in extracts of cerebral tissue, PCA demonstrated that metabolic deficits associated with NCL were greater than any effects produced from vitamin E supplementation. These deficits included increased glutamate and *N*-acetyl-L-aspartate and decreased creatine and glutamine concentrations in aqueous extracts of the cortex, as well as profound accumulation of lipid in intact cerebral tissue. This is discussed in terms of faulty production of mitochondrial-associated membranes, thought to be central to the deficits in *mnd* mice.

Batten's disease; motor neuron degeneration; metabolic profile; metabotype; neuronal ceroid lipofuscinosis; vitamin E

NEURONAL CEROID LIPOFUSCINOSES (NCL) are a series of autosomal recessive diseases, which together comprise the most common neurodegenerative disorders of childhood, with an incidence of 1 in 12,500 (30). The diseases are heterogeneous, based on four subtypes characterized by clinical pathology and age of onset and have been mapped to the gene loci CLN1 to CLN8 (2, 5, 10, 18, 21, 32, 37).

Article published online before print. See web site for date of publication (<http://physiolgenomics.physiology.org>).

Present address of J. L. Griffin and address for reprint requests and other correspondence: The Sanger Building, Department of Biochemistry, Tennis Court Road, University of Cambridge, CB2 1QW UK (E-mail: jlg40@mole.bio.cam.uk).

Despite the different gene loci, the diseases are typified by the accumulation of autofluorescent lipopigments in lysosomes, similar to the pigment lipofuscin, found in normal ageing brains (19, 31), and ceroid, found in pathological conditions (38), both formed by peroxidation of polyunsaturated fats. NCL diseases are also characterized by lysosomal abnormalities distinct to the individual forms (27), including the presence of inclusion bodies and the deposition of proteins such as subunit C of mitochondrial ATP synthase (13, 15, 27). Free radical generation is thought to take place at these inclusions sites, and as with motor neuron disease [amyotrophic lateral sclerosis (ALS)] and Parkinson's disease, peroxidation preferentially damages neuronal subgroups, producing the characteristic neurological degeneration. Although the complete biochemical processes that cause the NCLs are still to be defined, lipid handling, particularly within lysosomes, appears central to the disorders (10).

There has been a long-standing interest in the role of antioxidant molecules in diseases of the nervous system, and that failure of antioxidant protection is a common pathogenetic process in many neurodegenerative pathologies, including the NCL diseases. Decreased antioxidant levels have been reported in many neurological disorders, and on the basis of such evidence, antioxidant therapy has been used, in formal clinical trials but also widely as ad hoc dietary supplements by patients. The use of a model system that shows neurodegeneration in the presence of an antioxidant deficit allows the primary and secondary effects of the disease process and antioxidant deficit to be addressed.

The *mnd* mouse is a model of NCL (Batten's disease variant) (12, 20), with a mutation linked to the CLN8 gene (29). The model shows many of the characteristics of NCL, including retinal and neuronal degeneration and autofluorescent lipopigment in lysosomal storage pools (7). Vance and colleagues (34) have suggested that the transport of fats between the endoplasmic reticulum and mitochondria is impaired in these mice, implicating the involvement of defective mitochondrial-associated membranes (MAMs). In this study, we demonstrate biochemical abnormalities of the brain

and blood plasma using high-resolution proton nuclear magnetic resonance ($^1\text{H-NMR}$) spectroscopy and biochemical assay to metabolically profile the *mnd* mouse. By using such metabolic profiles to describe the dynamic phenotype of the *mnd* mouse during dietary supplementation, this study was able to investigate why, despite dietary supplementation of vitamin E reversing a detected deficiency of the vitamin in the *mnd* mouse, this did not reverse the pathological changes.

MATERIALS AND METHODS

Animal husbandry and procedures. *Mnd* and C57B6 control mice were maintained under standard conditions with food and water ad libitum. All procedures conformed to the UK Home Office regulations concerning the use of animals. Animals were kept in a constant environment with a 12:12-h light/dark cycle.

For biochemical assays two sets each of *mnd* and C57B6 control mice were fed on one of three diets [Special Diet Services (SDS)] after weaning (standard SDS1 is *diet 1*; SDS diet + 10 times vitamin E concentration is *diet 2*; and SDS diet + 10 times the concentration of vitamin E, vitamin C, and selenium is *diet 3*). Animals were killed by rising concentrations of carbon dioxide at 4 or 6 mo of age ($n = 6$ for each group). Brain tissue was rapidly dissected and frozen in liquid nitrogen, typically within 30 s postmortem. A terminal bleed was taken by cardiac puncture, and serum was separated by centrifugation.

For metabolic analysis using $^1\text{H-NMR}$ spectroscopy, two sets of *mnd* and control mice were fed one of the three diets described above ($n = 5$ for each group). Animals were killed at 6 mo of age by rising concentrations of carbon dioxide. Half the cerebral cortex was rapidly dissected and frozen using liquid nitrogen within 30 s. These samples were stored at 203 K. Additional samples were also collected from the remaining tissue and stored in 10% formal saline for histological analysis. Sera were collected as above and stored at 233 K.

Histology of brain tissue. Fixed cerebral samples were processed in paraffin wax using standard methods. Sections were cut at 10 μm thickness and stained with the Luxol-fast blue, Cresyl violet method to identify inclusion material more clearly.

Analysis of vitamin E and lipid content in brain tissue and blood plasma. Vitamin E content was determined using high-performance liquid chromatography (HPLC) with fluorometric detection using the method described by Buttriss and Diplock (4). Vitamin E concentrations were expressed in terms of cerebral tissue weight or ml of plasma.

Preparation of cerebral cortex extracts and NMR spectroscopy. Frozen tissue (~ 100 mg) was pulverized and added to 6% perchloric acid. The supernatant was neutralized with NaOH, lyophilized, and reconstituted in $^2\text{H}_2\text{O}$. Solutions were pipetted into 5-mm NMR tubes and analyzed using a spectrometer interfaced to a 14.1-Tesla magnet with a triple axis inverse geometry probe (model DRX 600; Bruker, Kahr-luhe, Germany). $^1\text{H-NMR}$ spectra were acquired using a standard presaturation pulse sequence based on the start of the nuclear Overhauser effect spectroscopy (NOESY) pulse sequence for water suppression (relaxation delay = 2 s, "mixing time" = 150 ms, time domain = 32 k data points, SW = 12 ppm, solvent presaturation applied during the relaxation delay and mixing time). After multiplication with an exponential function (equivalent to 0.3 Hz line broadening) and Fourier transformation of the free induction decays from

the time into the frequency domain, spectra were processed using XWIN-NMR (Bruker). Spectra were phased and baseline corrected using standard routines. To confirm spectral assignments made using literature values, gradient correlation spectroscopy (COSY), gradient heteronuclear single quantum coherence (HSQC), and two-dimensional J-resolved spectra were acquired using standard pulse programs.

Blood sera samples consisted of 300 μl of sera, 500 μl of sodium phosphate buffer (pH 7.1) and 100 μl of $^2\text{H}_2\text{O}$ (internal lock) with sodium-3-(trimethyl)- $^2\text{H}_4$ -propionate (TSP; final concentration 1 mM) as an internal reference standard ($\delta = 0.0$ ppm). Blood sera were analyzed by $^1\text{H-NMR}$ spectroscopy (256 acquisitions and 2-s interpulse delay) using a solvent suppressed pulse sequence with a total T_2 filter of 80 ms to attenuate broad signals from proteins and lipoproteins. Other acquisition parameters were as described above.

To further investigate cerebral tissue from *mnd* mice, intact cortical tissue from either *mnd* or control mice fed *diet 1* or *2* ($n = 4$; ~ 10 mg of tissue with ~ 5 μl of $^2\text{H}_2\text{O}$ acting as a frequency lock) were placed in a zirconium oxide rotors in a high-resolution magic angle spinning (HRMAS) probe, interfaced to the spectrometer described above. Samples were spun at 5,000 Hz at a temperature of 300 K. Initial $^1\text{H-NMR}$ spectra were acquired with 128 scans using the solvent suppressed sequence described above (total experimental time ~ 5 min). A sequential series of spectra were acquired every 30 min to monitor the degradation of *N*-acetyl-L-aspartate (NAA) to acetate. These changes were then fitted to a monoexponential to estimate the rate of degradation.

Pattern recognition of NMR spectra. For pattern recognition analysis, $^1\text{H-NMR}$ spectra were data reduced (AMIX v.2, Bruker) by subdivision into 0.04 ppm designated regions from δ 0.4–4.5. Each spectral region was normalized to the summation of spectral regions for the entire integral region of the spectrum, accounting for dilution or bulk mass differences between samples. Correlation principal components analysis (PCA) was performed using Pirouette v. 2.6 (Info-Metrix, Woodinville, WA) and SIMCA (Umea, Sweden). PCA is an unsupervised method of classification, requiring no training set of data, and hence is ideally suited to matrices with small group sizes, but large number of measurable parameters, correlating the variation detected in a data set to a spatial representation. The first PC generated by this method represents the maximum variation that is correlated, with subsequent PCs representing less variation and chosen to be orthogonal to the first PC.

Mean-centered, Pareto, and autoscaling routines were applied to the spectral data prior to PCA (11). Mean-centered analysis involved subtraction of the mean of the integral for a designated spectral region and PCA measures variance about this mean. Thus PCs in mean centered data are influenced by regions with the maximum variance about the mean. Autoscaled analysis sets each integral region to unit variance by scaling each region by $1/s_k$ where s_k represents the standard deviation of the variable k , following mean centering of the data set. This weights spectra so that features with lower spectral intensity and the high-concentration metabolites contribute equally to the PC analysis. Pareto scaling weights the integral regions to $(1/s_k)^{1/2}$ and results in an analysis midway between the other routines. Spectral data were reduced from 103 spectral descriptors to a number of PCs (typically less than 5), as determined by the maximization of cumulative total variation in the data that is predicted by those components. Loading plots from the PC analysis were used to identify metabolite (via their resonances) changes between groups. This was cross-validated

with spectra both visually and by manual integration of the regions.

Statistical analysis. Data are represented as means \pm standard deviation (SD) of the mean. Student's *t*-test (for two-way comparisons) and ANOVA test of variance with Tukey posttests were performed using InStat (Graphpad). To demonstrate the multiparametric analysis is also capable of identifying metabolite changes that were significantly different according to normal parametric tests, key metabolites were further investigated. For quoted metabolite ratios, integrals were calculated manually using Lorentzian line shapes to fit spectral resonances, and the ratios were compared using standard parametric tests.

RESULTS

Phenotype. Visual and gait disturbances were seen at 6 mo of age in all the *mnd* mice. No functional or behavioral differences were noted between groups of age-matched *mnd* mice, regardless of diet. Control mice showed no signs of ill health during the study.

Histology of brain tissue. Histological analysis was used to supplement observed phenotype, with the presence of intraneuronal inclusion material being constantly associated with the *mnd* phenotype. Neuronal inclusion material was present as eosinophilic masses within the cytoplasm on hematoxylin and eosin staining and stained positively with the Luxol fast blue/Cresyl violet method (Fig. 1). Inclusions were seen in most neuronal groups but were most evident in large neurons, such as pyramidal neurons of the cerebral cortex. No differences were noted in the amount or distribution of inclusion material between *mnd* mice of the same age on *diet 1*, *2*, or *3*. Tissue from control mice had no abnormal histological features in any group.

Vitamin E content of tissues. At 4 mo *mnd* mice had decreased vitamin E content in brain tissue compared with control animals (Fig. 2) according to an ANOVA test followed by Tukey posttesting, with this deficit increasing by 6 mo ($P < 0.05$ for difference between *mnd* and control mice fed *diet 1* at 4 and 6 mo).

Dietary supplementation of vitamin E increased its content to above control levels in sera for both mice strains, with content rising approximately two- and threefold in control and *mnd* mice at 6 mo, respectively ($P < 0.05$ for increase in vitamin E content in *mnd* mice on *diet 2* compared with *diet 1* at 4 and 6 mo). Supplementation of vitamin E in *mnd* mice increased vitamin E content above that found in control mice on the normal diet for both sera and cerebral tissue, indicating the vitamin E deficiency was reversed.

Serum metabolic profiles. The spectral profiles of sera from *mnd* mice (Fig. 3, A and B) showed a number of metabolic perturbations compared with control animals and were separated using PC analysis. For a comparison between all *mnd* mice and control mice, regardless of diet, this separation was represented by PC 1 and PC 2, accounting for 66.3% of the total spectral variation (Fig. 3C). Lactate, CH_3CH_2- lipid moieties and glucose were all decreased in *mnd* mouse serum whereas $\text{CH}_2\text{CH}_2\text{CH}_2$ lipid moieties were relatively increased (Fig. 3D). (Note: here and throughout, boldface indicates "resonance observed.")

Supplementation of vitamin E to the diet of *mnd* mice caused a decrease in the resonance intensities of lipid polyunsaturated groups in the sera spectra, especially at δ 2.78 associated with $\text{C}=\text{CCH}_2\text{C}=\text{C}$ moieties. Manual integration of this peak and expressing it as a ratio with the lactate resonance, at δ 1.33 indicated a twofold relative decrease (*diet 1* = 0.095 ± 0.017 , *diet 2* = 0.050 ± 0.005 , $P < 0.05$; Student's *t*-test). However, this change was not observed in control animals. In addition to this difference, spectral profiles of *mnd* mouse blood plasma indicated increased $\text{CH}_2\text{CH}_2\text{CH}_2$ lipid moieties and a general decrease in glucose resonances compared with blood plasma from control animals also fed on *diet 2*. The relative ratio of the integrals of the glucose resonance at δ 3.42 and the $\text{CH}_2\text{CH}_2\text{CH}_2$ lipid moiety at δ 1.30 showed a greater than twofold decrease between

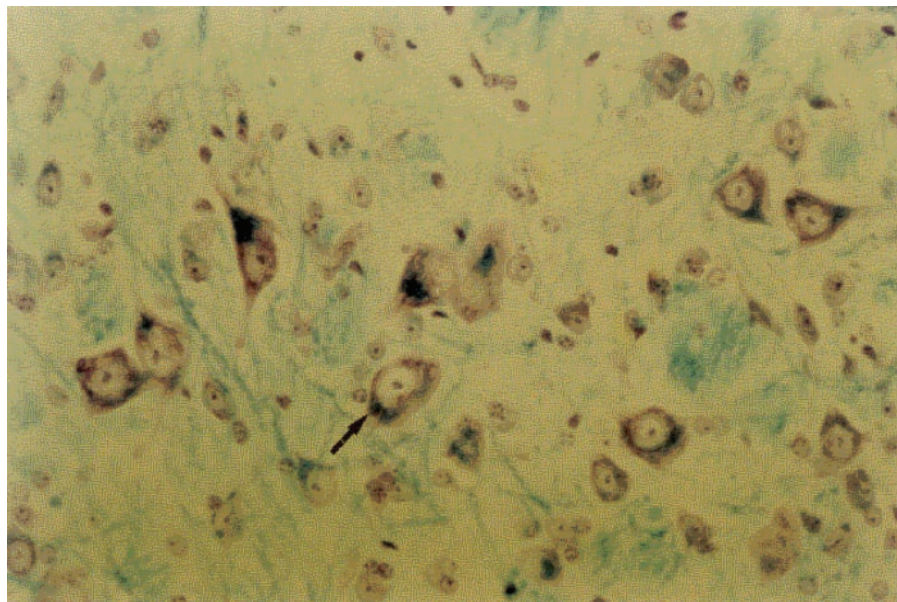


Fig. 1. Luxophilic cytoplasmic inclusion bodies in the cerebral cortex of the *mnd* mouse: Luxol fast blue and Cresyl violet staining; magnification, $\times 100$. Arrow shows an inclusion body. No inclusions bodies were found in cerebral tissue of control mice, whereas all cerebral tissue from *mnd* mice had inclusion bodies, regardless of diet.

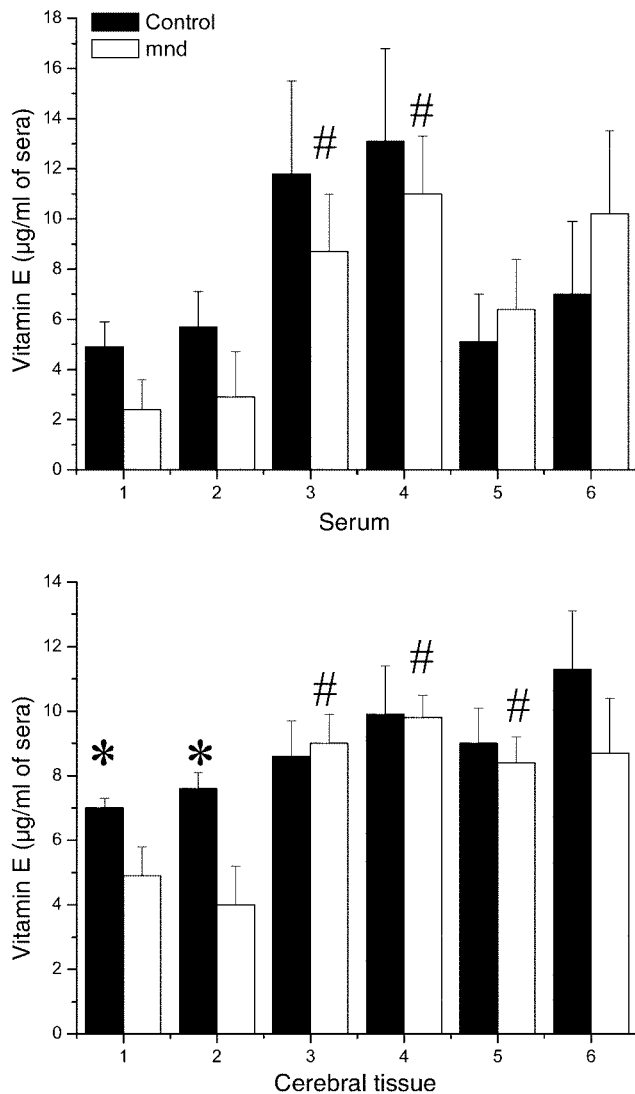


Fig. 2. Vitamin E content in sera (top) and cerebral cortex (bottom) of the *mnd* mouse. By means of an ANOVA test of variance, vitamin E content was found to be significantly altered across the three diets, two age groups, and two mouse strains investigated for both sera and cerebral tissue ($P < 0.0001$). Selected Tukey posttests were then applied. Data are means \pm SD ($n = 6$). Odd numbers indicate 4-mo-old animals, even numbers are for 6-mo-old animals, for diet 1 (1 and 2), diet 2 (3 and 4), and diet 3 (5 and 6). * $P < 0.05$ for Tukey posttest for difference between *mnd* and control mice at the same age and on the same diet. # $P < 0.05$ for difference between *mnd* mice on diet 1 and either diet 2 or diet 3 for same age mice.

mouse types ($P < 0.01$ for Student's *t*-test). These differences were also apparent in the two mice groups fed diet supplemented with vitamins E and C and selenium (diet 3).

For all comparisons the metabolic changes caused by gene expression were greater than those caused by diet. Thus the metabolic profiles of sera from *mnd* mice were metabolically perturbed, and sera glucose concentrations in all three groups of *mnd* mice were reduced. Vitamin E supplementation reduced the concentration of serum unsaturated fatty acids in *mnd* mice but failed to correct the other metabolic deficits detected.

Cerebral metabolic profiles. Cerebral cortex tissue extracts (Fig. 4) from *mnd* mice were readily separated according to PC analysis, following all the preprocessing routines, regardless of diet (Fig. 5A). To further investigate the biochemical differences present within the cerebral tissue of *mnd* mice, the individual diet groups were investigated alongside their control siblings. *Mnd* and control mice were separated in PC analysis along PC 1, representing the maximum variance in the data set (Fig. 5B; 30.2% of the variance for Pareto scaled data; $P < 0.05$ for difference in PC loading). Examining the contribution plots, this was caused by increased β -hydroxybutyrate (δ 1.22), taurine (δ 3.26), and glutamate (δ 2.12, 2.36) and decreased creatine (δ 3.02), aspartate (δ 2.88), glutamine (δ 2.20), and GABA (δ 1.84) tissue content (Fig. 5E). Pattern recognition was applied only to the aliphatic region of the spectrum, because of variability in water suppression, but in the spectra from *mnd* mouse tissue phenylalanine was also present (Fig. 4B).

Supplementing the diet with extra vitamin E reduced the concentration of phenylalanine dramatically in extracts of *mnd* brain [relative ratio of phenylalanine (δ 7.42)/lactate (δ 1.33) in normal diet = 0.059 ± 0.026 ; with vitamin E = 0.006 ± 0.003 ; $P < 0.005$ for *t*-test with Welch correction]. The dietary supplementation also decreased cerebral concentrations of β -hydroxybutyrate [Fig. 4C; ratio of β -hydroxybutyrate (δ 1.22)/lactate (δ 1.33) normal diet = 0.085 ± 0.017 ; with vitamin E = 0.004 ± 0.002 , $P < 0.005$ for *t*-test with Welch correction] and glutamate. However, PC analysis demonstrated that the metabolic profiles of *mnd* mice fed diet 2 were distinct from control mice fed either diet 1 or 2 (Fig. 5B). Again, this separation was caused by decreases in concentration of creatine (δ 3.02), aspartate (δ 2.88), and glutamine (δ 2.20) and an increase in glutamate (δ 2.36, 2.14), and β -hydroxybutyrate (δ 1.24), as well as an increase in concentration of lactate (δ 1.33) and NAA (δ 2.0) (Fig. 5F). Supplementation of the diet with vitamins E and C as well as selenium (diet 3) produced spectral profiles similar to that observed during simple vitamin E supplementation alone, and animals fed either diet 2 or 3 could not be separated by PCA alone for one particular strain (Fig. 5C). Thus, despite vitamin E supplementation reversing the cerebral deficit in vitamin E, *mnd* mice had a metabolic profile distinct from control animals, and this perturbation was larger than the effect associated with diet. The key metabolite changes are summarized in Table 1.

No common biochemical effect was detected by PCA for both mouse strains attributable to vitamin E supplementation, until the data set was preprocessed using orthogonal signal correction (OSC; 20), indicating that the biochemical abnormalities associated with NCL were far greater than the changes induced by vitamin E supplementation. OSC removes variation not correlated with a Y variable. Following OSC, to separate variation not correlated to vitamin E content within the tissue (removing 67% of the variation in the data set over two PLS components), the spectra from

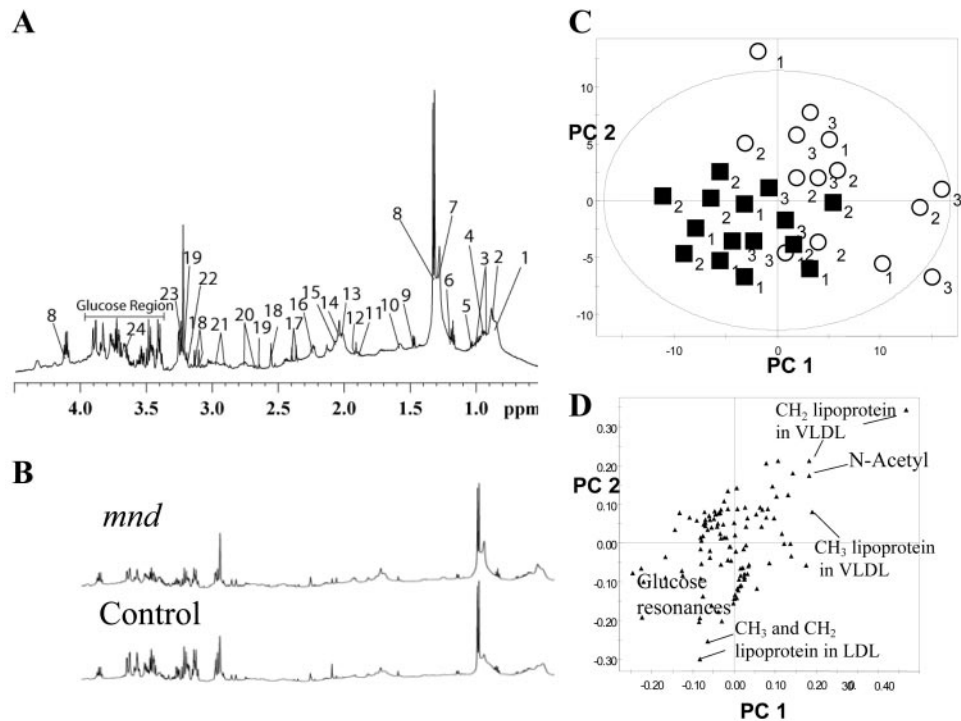


Fig. 3. A: 600.13 MHz high-resolution ^1H -NMR spectrum of blood sera from a *mnd* mouse fed *diet 1*. (Note: boldface indicates “resonance observed.”) *Peak 1*, CH_3CH_2 low-density lipids (LDL); *peak 2*, CH_3CH_2 very low-density lipids (VLDL); *peak 3*, isoleucine; *peak 4*, leucine; *peak 5*, valine; *peak 6*, ethanol; *peak 7*, $\text{CH}_2\text{CH}_2\text{CH}_2$ VLDL and LDL; *peak 8*, lactate; *peak 9*, alanine; *peak 10*, COCH_2CH_2 ; *peak 11*, lysine + arginine; *peak 12*, acetate; *peak 13*, $-\text{CH}_2-\text{C}=\text{C}-$; *peak 14*, *N*-acetyl glycoproteins; *peak 15*, *N*-acetyl glycoproteins; *peak 16*, $-\text{CH}_2\text{CO}$ lipids; *peak 17*, EDTA; *peak 18*, calcium EDTA^{2-} ; *peak 19*, magnesium EDTA^{2-} ; *peak 20*, $-\text{C}=\text{C}-\text{CH}_2-\text{C}=\text{C}$ lipids; *peak 21*, albumen lysyl groups; *peak 22*, choline; *peak 23*, C_2H β -glucose; *peak 24*, glycerol. B: comparison between spectra obtained from *mnd* and control mouse sera to demonstrate the reduction in glucose-containing resonances in the plasma from *mnd* mice. C: principal component analysis (PCA) of sera spectra from the two mouse strains and three diets. Plasma from *mnd* mice had a distinct metabolic profile compared with control animals regardless of diet. Numbers indicate diet; \blacksquare , control spectra; \circ , *mnd* mice. D: loadings plot to show metabolites that contribute most to this separation. Metabolites found in the *top right* are increased and those in the *bottom left* are decreased in spectra of *mnd* mouse sera.

animals receiving supplemented vitamin E in their diets were separated in PCs 2 and 3 (Fig. 5e), with the OSC weighted loadings being affected most by the relative ratios of alanine to creatine and alanine to aspartate (increased during vitamin E supplementation). However, the low goodness of fits (R^2) for PCs 2 and 3 indicated that this trend was weak.

In summary, vitamin E supplementation reduced the high concentrations of phenylalanine and β -hydroxybutyrate detected in cerebral tissue of *mnd* mice but did not fully restore the abnormal concentrations of other low-molecular-weight metabolites including glutamate, glutamine, aspartate, and creatine within cerebral tissue from *mnd* mice.

Intact cerebral cortical tissue. Using high-resolution MAS ^1H -NMR spectroscopy, spectral profiles were obtained of *mnd* and control mice fed *diets 1* and *2*. Tissue from *mnd* mice clearly had increased lipid content, with the $\text{CH}_2\text{CH}_2\text{CH}_2$ resonance being particularly prominent (δ 1.3 ppm) (Fig. 6A). Unlike tissue obtained from control animals, tissue from *mnd* mice also had a visible resonance associated with $\text{CH}=\text{CH}$ lipid moieties at 5.6 ppm. Application of PCA to the intact spectra readily separated tissue from control and

mnd mice along PC 1 ($P < 0.005$ for difference between strains), and this was largely caused by the $\text{CH}_2\text{CH}_2\text{CH}_2$ lipid resonance, confirming the changes detected visually. Similar lipid deposits were detected in spectra from *mnd* mice fed *diet 2*, and PCA failed to separate the mice according to diet for either strain.

While initial spectra were acquired within 15 min of sample preparation (the time for shimming and acquisition), NAA degradation to acetate occurred during the acquisition. As NAA was highlighted as one of the perturbed metabolites in the PC analysis of cerebral tissue extracts, the degradation rate of NAA and the rate of formation of acetate was measured by sequentially acquiring spectra every 30 min (each spectrum required a 5-min acquisition and a 25-min delay prior to the next acquisition), to test the hypothesis that NAA degradation was slower in *mnd* mice (Fig. 6B). Measuring both the direct rate and the rate of accumulation of acetate, degradation of NAA was slower in tissue from *mnd* mice compared with that from control animals (*mnd*, $v_{\text{NAA}} = -0.0018 \pm 0.0002/\text{min}$; control, $v_{\text{NAA}} = -0.0022 \pm 0.0001/\text{min}$; $P = 0.0059$ for Student's *t*-test).

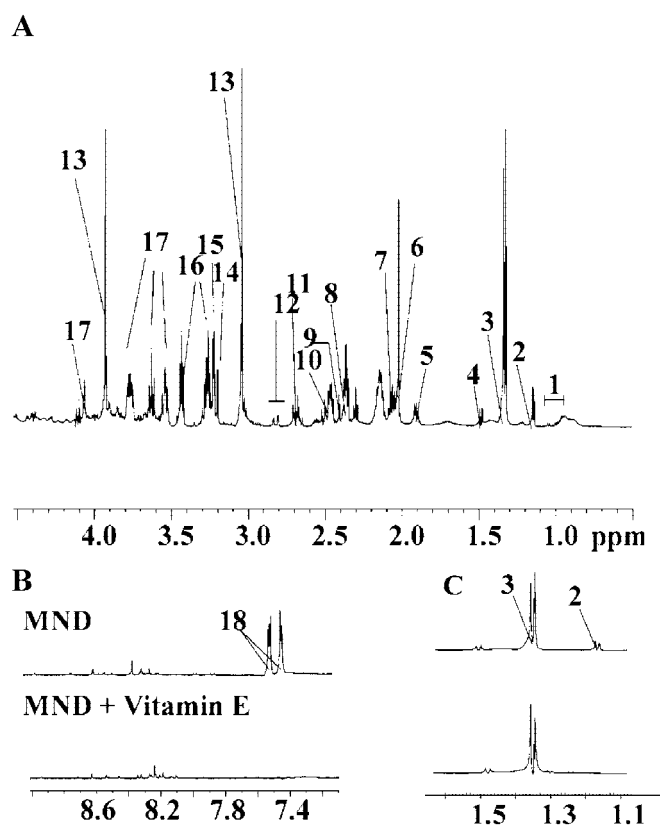


Fig. 4. A: 600.13 MHz high-resolution $^1\text{H-NMR}$ spectrum of a perchloric acid extract of cortex tissue from the *mnd* mouse. Peak 1, valine, leucine, isoleucine; peak 2, β -hydroxybutyrate; peak 3, lactate; peak 4, alanine; peak 5, γ -aminobutyric acid (GABA); peak 6, *N*-acetyl-L-aspartate (NAA); peak 7, glutamate and glutamine; peak 8, glutamate; peak 9, succinate; peak 10, glutamine; peak 11, hypotaurine and aspartate; peak 12, aspartate; peak 13, creatine; peak 14, choline; peak 15, phosphocholine; peak 16, taurine; peak 17, myo-inositol (and smaller contributions from glycine, α protons of amino acids and glucose); and peak 18, phenylalanine. B and C: enlargements of ^1H spectra from *mnd* mice on diets 1 and 2 showing main differences between spectral profiles.

DISCUSSION

Vitamin E is decreased in mnd tissue. Free radical damage is implicated in the different forms of NCL as well as other neurodegenerative diseases, including Parkinson's disease and ALS. Highly reactive OH radicals oxidize unsaturated fatty acids within cell membranes, forming lipid hydroperoxides and disrupting cell membrane integrity and fluidity. The high redox reactivity, coupled with cell membranes rich in polyunsaturated fatty lipids, predispose neuronal tissues, especially motor neurons, to free radical damage. It has been suggested that dietary supplementation with antioxidants may reverse the pathologies of these diseases (3, 17, 33).

The concentration of vitamin E is reduced in cerebral tissue and blood plasma from *mnd* mice, and features of primary vitamin E deficiency include a number of neurological symptoms, such as ataxia, loss of proprioception and deep tendon reflexes, and retinal damage (22). However, the concentration of vitamin E in *mnd*

mice fed on a non-supplemented diet was greater than those reported in deficiency disorders. Furthermore, the deficit in vitamin E concentration was reversed by dietary supplementation, but this did not prevent the progression of cerebral disorders in *mnd* mice. Histology confirmed that cerebral tissue had characteristic lesions, similar to those found in human patients of NCL (30), in all groups of *mnd* mice studied, with no differences in the quantity or distribution of inclusion material regardless of diet. In the present study we have used $^1\text{H-NMR}$ spectroscopy of cerebral tissue extracts and intact tissue to directly study which metabolic abnormalities could and could not be corrected by vitamin E supplementation, by defining a metabolic phenotype for each treatment group.

Metabolic profiles of mnd mice are distinct from control mice. The decreased sera concentrations of glucose and lactate accompanied by an increase in the ratio of $\text{CH}_2\text{CH}_2\text{CH}_2/\text{CH}_2\text{CH}_3$ lipid moieties indicate a perturbation between carbohydrate and lipid metabolism, further supported by the large concentration of β -hydroxybutyrate detected in cerebral tissue, a known consequence of prolonged starvation and non-insulin-dependent diabetes (25). However, the concentration of β -hydroxybutyrate present within blood sera was small for both groups (unlike during starvation; 25), typically obscured by other resonances, and no differences in animal weights or food intake between groups were noted. Instead these changes are characteristic of a profound metabolic disorder in terms of glucose management, such as occurs during non-insulin-dependent diabetes.

Striking differences were detectable in spectra from intact tissue, with *mnd* mice possessing a high concentration of $\text{CH}_2\text{CH}_2\text{CH}_2$ lipid moieties, just as detected in sera. The spectral profiles from *mnd* tissue also had a pronounced resonance associated with $\text{CH}=\text{CH}$ lipid moieties, primary sites of free radical attack, as well as being associated with apoptosis in tumors of the brain (14). Thus the lipid profile of cortical tissue from *mnd* mice demonstrates characterizable metabolic deficits consistent with an abnormality in lipid metabolism, such as caused by faulty production of MAMs, as suggested by Vance and coworkers (34). Impaired formation of MAMs is thought to cause a redistribution of MAM-associated enzymes, including a number involved in lipid metabolism, such as phosphatidylethanolamine *N*-methyltransferase-2, CTP:phosphocholine cytidyltransferase, and phosphatidylserine synthase. Defective membrane formation has also been implicated in juvenile NCL, both in terms of total phosphatidylcholine, phosphatidylserine, and phosphatidylethanolamine in erythrocytes and platelets, and impaired Ca^{2+} mobilization in fibroblasts (2, 3). Peroxide damage then arises because of reduced transport of lipids between the endoplasmic reticulum and the mitochondria. Disruptions in lipid metabolism, particularly events associated with lysosomes, appear common to all the NCL-related disorders (3, 10, 16, 35–36).

The low-molecular-weight metabolites also provided a unique insight into the disease process. Phenylala-

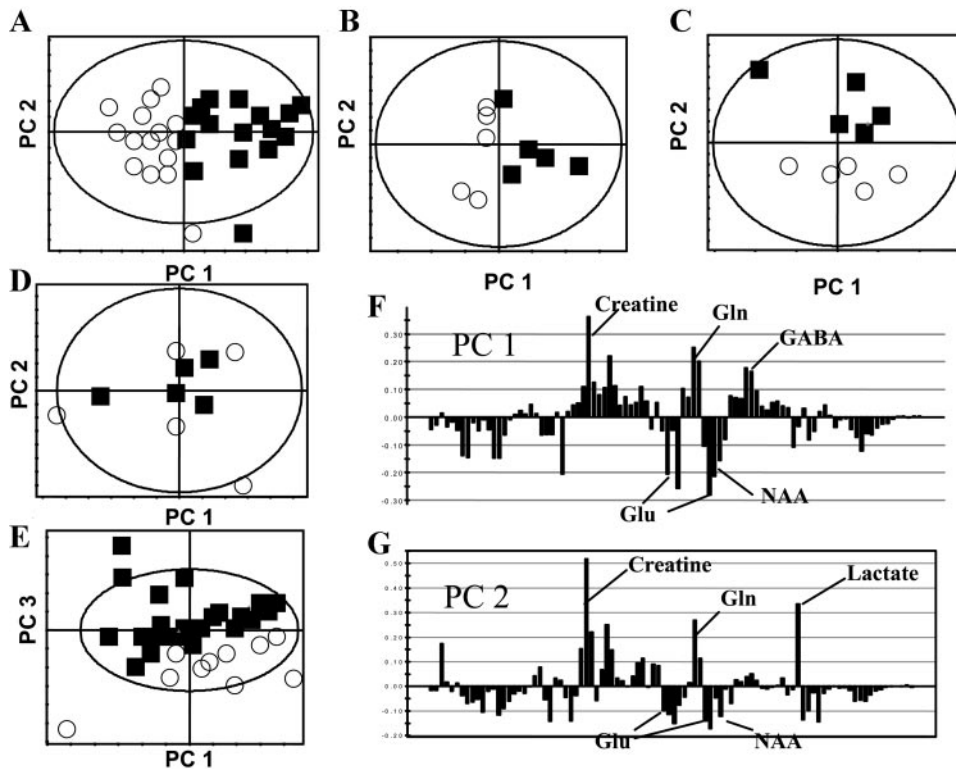


Fig. 5. Representative PCA of perchloric acid extract of cerebral cortex tissue. All plots are derived from Pareto scaled data and represent the following spectral comparisons (A–E). A: all *mnd* (○) and control mice (■). B: *mnd* (○) and control mice (■) fed diet 1. C: *mnd* (○) and control mice (■) fed diet 2. D: *mnd* mice fed diet 2 (○) or diet 3 (■). E: OSC filtered data of all mice fed diet 1 (○) or diet 2 or 3 (■) (see RESULTS for explanation of preprocessing routine). F: contributions plot for the separation of *mnd* and control mice fed diet 1 (see B for PC loadings). The x-axis represents the different 0.04 ppm integral regions used as metabolic descriptors (arranged to reflect a NMR spectrum), whereas the y-axis measures the importance of the contribution of each metabolite. Key metabolites having a negative score in this PC (i.e., decreased creatine, glutamine, etc., but increased glutamate and NAA). G: contributions plot for cerebral tissue of *mnd* and control mice fed diet 2.

nine was detected in cerebral tissue of *mnd* mice, with a host of neurological pathologies, including phenylketouria, characterized by impaired metabolism of phenylalanine and hence a failure to maintain tyrosine and dopamine concentrations within cerebral tissue (23). This deficit could be corrected by supplementation with vitamin E. However, regardless of diet, concentrations of lactate, glutamate, and NAA were all increased in *mnd* cerebral tissue, whereas that of creatine, glutamine, aspartate, and GABA were decreased, and these differences were more pronounced than

Table 1. Major metabolite differences between control and *mnd* mice fed diet 1 and *mnd* mice fed diet 2

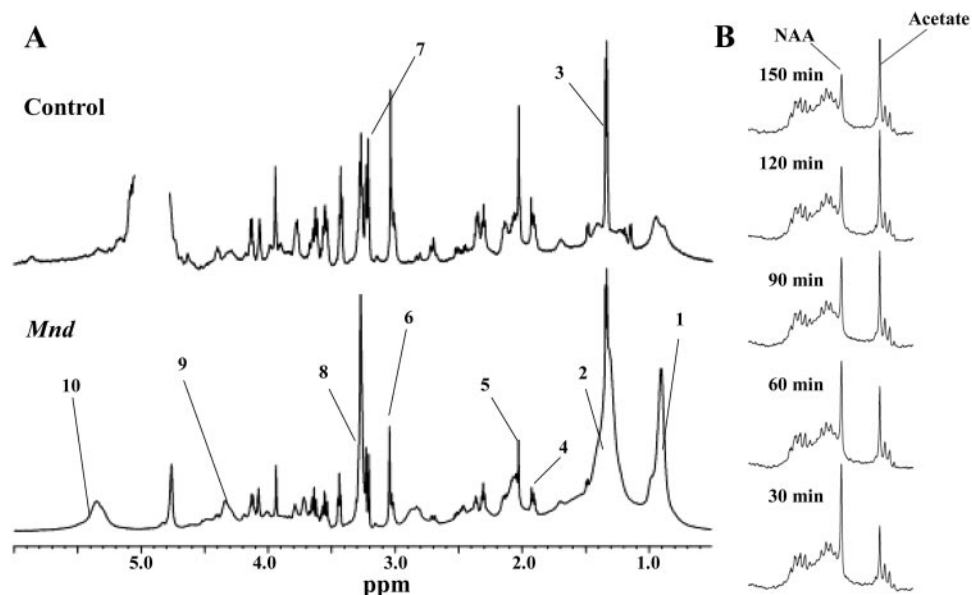
	Control and <i>mnd</i> Mice Fed Diet 1	<i>Mnd</i> Mice Fed Diets 1 or 2
Blood plasma	CH₂CH₂CH₂ lipid (+) Lactate (–) CH₃CH₂ - lipid (–) Glucose (–)	C=CH₂C=C lipid (–)
Cerebral extracts	β -hydroxybutyrate (+) taurine (+) glutamate (+) phenylalanine (+) creatine (–) aspartate (–) glutamine (–) GABA (–)	β -hydroxybutyrate (–) phenylalanine (–)

Key metabolite changes were identified by multiparametric analysis using the automated integral data set or using standard parametric tests following manual integration of resonances; + and – indicate either an increase or decrease in metabolite concentration in either *mnd* mice, or induced by diet 2 for columns 2 and 3, respectively. Chemical groups in boldface indicate resonance observed.

those induced by dietary supplementation. GABAergic interneurons are selectively lost in mouse models of NCL and infantile NCL (8, 9) explaining the decrease in GABA detected. However, the increase in neuronal markers NAA and glutamate at the expense of creatine and glutamine, glial markers of metabolism, in *mnd* cerebral tissue is counterintuitive for a disease that primarily affects motor neurons. Vance and colleagues (34), studying enzyme expression in liver tissue from *mnd* mice, made the observation that while certain enzymes were decreased in concentration in the MAMs, their expression in the overall tissue was the same as control tissue, suggesting a redistribution of the enzymes. Thus the distribution of metabolites across intracellular compartments may be altered within cerebral tissue from *mnd* mice.

Tissue removal takes a finite amount of time, particularly where tissue sections are also taken for histology, preventing the use of such techniques as funnel freezing. The slower degradation of NAA in cerebral tissue from *mnd* mice suggests that the actual concentration of NAA was the same in both mouse strains at the time of death, but differences were caused by different degradation rates. This may be caused by impaired transport of the metabolite from its production in the mitochondria to where it is metabolized, presumably connected to defective MAMs production. This is intriguing, as although the exact metabolic purpose of NAA is still disputed, it has been suggested to be a precursor in myelin production or involved in water homeostasis, with both events involving oligodendrocytes, providing a link between NAA degradation, lipid

Fig. 6. A: 600.13 MHz high-resolution magic angle spinning ^1H -NMR spectra of intact cortical tissue from a *mnd* and control mouse. Tissue from the *mnd* mice with resonances at 1.30 ppm (long-chain alkane groups) and 5.35 ppm (unsaturated lipid moieties). Peak 1, CH_3CH_2 lipid groups; peak 2, $\text{CH}_2\text{CH}_2\text{CH}_2$ lipid groups; peak 3, lactate; peak 4, acetate; peak 5, NAA; peak 6, creatine; peak 7, choline and phosphocholine; peak 8, phosphatidylcholine; peak 9, glycerol; and peak 10, $\text{CH}=\text{CH}$ lipid groups. B: degradation of NAA to acetate at 300 K in a piece of intact cortical tissue from a control mouse.



metabolism/transport, and metabolism within glia (1, 6). The neurological disorders associated with the disruption of the CLN8 gene appear connected with these metabolic differences, as despite the ability of vitamin E to correct the concentration of phenylalanine within the tissue, there was no effect on observational or histopathological phenotype. Although NAA is decreased in human sufferers of juvenile NCL, presumably this is a result of significant neuronal cell loss in this more progressive form and hence not a primary marker of the disease process.

Vitamin E supplementation did not correct all metabolic abnormalities. Supplementation of the diet with vitamin E reversed the detected deficit in vitamin E in *mnd* mice, increasing cerebral and blood sera concentrations to above control values. However, none of the resultant metabolic changes were as great as the primary metabolic deficit associated with NCL. With PC analysis of the sera and cortical tissue data sets, spectra from *mnd* and control mice could always be separated regardless of diet. Indeed, to determine the effects of vitamin E, either a two-group comparison or a data filtration technique such as OSC was necessary (11). In all cases, vitamin E was not directly detected in the NMR spectra (even in the most oxidative environments, such as the mitochondrial membrane, vitamin E concentration is 1:500 relative to lipids; 4). Hence, all the changes detected arose from the biochemical effects of the vitamin rather than its direct effects on the spectra.

Diet 2 caused a decrease in unsaturated fatty acids circulating in blood in *mnd* mice but not control mice. As vitamin E is expected to decrease peroxidation of unsaturated fats, a decrease in circulating polyunsaturated fats in the *mnd* mice suggests that there is a decrease in turnover of these metabolites in the tissues of the body, caused by decreases in peroxidation of membranes, particularly mitochondrial. Despite this change induced by vitamin E supplementation, lactate

and glucose remained decreased in the blood plasma of *mnd* mice fed *diet 2* or *3*, and the changes in lipid resonances suggested that sera from *mnd* mice contained longer chain fatty acids than in control animals (i.e., increased $\text{CH}_2\text{CH}_2\text{CH}_2$ resonance intensities), just as in the mice fed *diet 1*.

In this study two antioxidant-supplemented diets were used. Vitamin C is water soluble, but it has been suggested that it may be involved in regenerating vitamin E (26), while selenium is a constituent of glutathione peroxidase, which reduces peroxides. However, in both serum and cerebral tissue no metabolic differences were detected between the two diets, with metabolic changes being most pronounced in the vitamin E supplemented *diet 2*.

Conclusion. With increasing number of genetically modified organisms, it is becoming apparent that new phenotyping techniques are necessary to explore the functional genomics of a given gene deletion or modification. This has led to the emergence of metabolic profiling techniques reliant on NMR spectroscopy or mass spectrometry referred to as “metabonomics” or “metabolomics” (24, 28). This approach is illustrated in this study by the *mnd* mouse, whose phenotype is characterized by a reduction in cerebral and sera concentrations of vitamin E, although reversal of this deficit failed to prevent the pathological effects associated with NCL. Deriving metabolic profiles, using a technique such as high-resolution ^1H -NMR spectroscopy, a metabolic phenotype was produced determining the pathways corrected and uncorrected by vitamin E supplementation. Such an approach should be equally applicable to any animal model of disease, providing a rapid and convenient way to predict metabolic phenotypes.

This work is supported by the Motor Neuron Disease Association, the Special Trustees of the Royal London Hospital, The Annie Lindsell Trust, and the Birth Defects Foundation. J. L. Griffin is grateful

for the University Research Fellowship awarded by the Royal Society and for useful discussions with Dr. Ned Mason.

REFERENCES

1. **Baslow MH.** Evidence supporting a role for *N*-acetyl-L-aspartate as a molecular water pump in myelinated neurons in the central nervous system: an analytical review. *Neurochem Int* 40: 295–300, 2002.
2. **Bennett MJ, Gayton AR, Rittey CDC, and Hosking GP.** Juvenile neuronal ceroid-lipofuscinosis: developmental progress after supplementation with polyunsaturated fatty acids. *Dev Med Child Neurol* 36: 630–638, 1994.
3. **Bennett MJ and Hoffmann SL.** The neuronal ceroid-lipofuscinoses (Batten disease): a new class of lysosomal storage diseases. *J Inherit Metab Dis* 22: 535–544, 1999.
4. **Buttriss JL and Diplock AT.** High performance liquid chromatography methods for vitamin E in tissues. *Methods Enzymol* 105: 131–138, 1983.
5. **Carpenter S, Karpati G, Andermann F, Jakob JC, and Andermann E.** The ultrastructural characteristics of the abnormal cytosomes in Batten-Kufs' disease. *Brain* 100: 137–156, 1977.
6. **Chakraborty G, Mekala P, Yahya D, Wu G, and Ledeen RW.** Intraneuronal *N*-acetylaspargate supplies acetyl groups for myelin lipid synthesis: evidence for myelin-associated aspartoacylase. *J Neurochem* 78: 736–745, 2001.
7. **Chang B, Bronson RT, Hawes NL, Roderick TH, Peng C, Hageman GS, and Heckenlively JR.** Retinal degeneration in motor neuron degeneration: a mouse model of ceroid lipofuscinosis. *Invest Ophthalmol Vis Sci* 35: 1071–1076, 1994.
8. **Cooper JD, Messer A, Feng AK, Chua-Couzens J, and Mobley WC.** Apparent loss and hypertrophy of interneurons in a mouse model of neuronal ceroid lipofuscinosis: evidence for partial response to insulin-like growth factor-1 treatment. *J Neurosci* 19: 2556–2567, 1999.
9. **Cooper JD, Gupta B, Bible E, Hofmann S, and Lantos S.** Profound loss of GABAergic interneurons in the PPT1 knockout mouse model of infantile neuronal ceroid lipofuscinosis. *Neuropathol Appl Neurobiol* 28: 158–159, 2002.
10. **Dawson G and Cho S.** Batten's disease: clues to neuronal protein catabolism in lysosomes. *J Neurosci Res* 60: 133–140, 2000.
11. **Eriksson L, Johansson E, Kettaneh-Wold N, and Wold S.** *Introduction to Multi- and Megavariate Data Analysis using Projection Methods (PCA & PLS)*. Umea, Sweden: Umetrics, 1999.
12. **Faust JR, Rodman JS, Daniel PF, Dice F, and Bronson RT.** Two related proteolipids and dolichol-linked oligosaccharides accumulate in motor neuron degeneration mice (mnd/mnd), a model for neuronal ceroid lipofuscinosis. *J Biol Chem* 269: 10150–10155, 1994.
13. **Fearnley IM, Walker JE, Martinus RD, Jolly RD, Kirkland RB, Shaw GJ, and Palmer DN.** The sequence of the major protein stored in ovine ceroid lipofuscinosis is identical to that of the DCCD-reactive proteolipid mitochondrial ATP synthase. *Biochem J* 268: 751–758, 1990.
14. **Hakumaki JM and Kauppinen RA.** ¹H-NMR visible lipids in the life and death of cells. *Trends Biochem Sci* 25: 357–362, 2001.
15. **Hall NA, Lake BD, Dewji NN, and Patrick AD.** Lysosomal storage of subunit C of mitochondrial ATP synthase in Batten disease (ceroid lipofuscinosis). *Biochem J* 275: 269–272, 1991.
16. **Hoffman SL, Atashband A, Cho SK, Das AK, Gupta P, and Lu JY.** Neuronal ceroid lipofuscinoses caused by defects in soluble lysosomal enzymes (CLN1 and CLN2). *Curr Mol Med* 2: 423–37, 2002.
17. **Katz ML, Rice LM, and Gao C.** Dietary carnitine supplements slow disease progression in a putative mouse model for hereditary ceroid-lipofuscinosis. *J Neurosci Res* 57: 551–556, 1997.
18. **Klockars T, Savukoski M, Isosompii J, and Peltonen L.** Positional cloning of the CLN5 gene defective in the Finnish variant of the LINCL. *Mol Genet Metab* 66: 324–328, 1999.
19. **Mann DM, Yates PO, and Stamp JE.** The relationship between lipofuscin pigment and ageing in the human nervous system. *J Neurol Sci* 37: 83–93, 1978.
20. **Messer A and Flaherty L.** Autosomal dominance in a late onset motor neuron disease in the mouse. *J Neurogenet* 3: 345–355, 1986.
21. **Mole S and Gardiner M.** Molecular genetics of the neuronal ceroid lipofuscinoses. *Epilepsia* 40: 29–32, 1999.
22. **Muller DPR and Goss-Sampson MA.** Neurochemical, neurophysiological, and neuropathological studies in vitamin E deficiency. *Crit Rev Neurobiol* 5: 239–263, 1990.
23. **Newsholme EA and Leech AR.** *Biochemistry for the Medical Sciences*. Chichester, UK: Wiley, 1994.
24. **Nicholson JK, Connelly J, Lindon JC, and Holmes E.** Metabonomics: a platform for studying drug toxicity and gene function. *Nat Rev Drug Discov* 1: 153–161, 2002.
25. **Owen OE, Morgan AP, Kemp HG, Sullivan JM, Herrera MG, and Cahill GF Jr.** Brain metabolism during fasting. *J Clin Invest* 46: 1589–1595, 1967.
26. **Packer L and Landvik S.** Vitamin E in biological systems. *Adv Exp Med Biol* 264: 93–106, 1990.
27. **Palmer DN, Fearnley IM, Walker JE, Hall NA, Lake BD, Wolfe LS, and Haltia M.** Mitochondrial ATP synthase subunit c storage in the ceroid-lipofuscinoses (Batten disease). *Am J Med Genet* 42: 561–567, 1992.
28. **Raamsdonk LM, Teusink B, Broadhurst D, Zhang N, Hayes A, Walsh MC, Berden JA, Brindle KM, Kell DB, Rowland JJ, Westerhoff HV, van Dam K, and Oliver SG.** A functional genomics strategy that uses metabolome data to reveal the phenotype of silent mutations. *Nat Biotechnol* 19: 45–50, 2001.
29. **Ranta S, Zhang Y, Ross B, Lonka L, Takkunen E, Messer A, Sharp J, Wheeler R, Kusumi K, Mole S, Liu W, Soares MB, Bonaldo MF, Hirvasniemi A, de la Chapelle A, Gilliam TC, and Lehesjoki AE.** The neuronal ceroid lipofuscinoses in human EPMR and mnd mutant mice are associated with mutations in CLN8. *Nat Genet* 23: 233–236, 1999.
30. **Santavuori P.** Neuronal ceroid-lipofuscinoses in childhood. *Brain Dev* 10: 80–83, 1988.
31. **Sekhon SS and Maxwell DS.** Ultrastructural changes in neurons of the spinal anterior horn of ageing mice with particular reference to the accumulation of lipofuscin pigment. *J Neurocytol* 3: 59–72, 1974.
32. **Sharp JD, Wheeler RB, Lake BD, Fox M, Gardiner RM, and Williams RE.** Genetic and physical mapping of the CLN6 gene on chromosome 15q21–23. *Mol Genet Metab* 66: 329–331, 1999.
33. **Siakotos AN, Koppang N, Youmans S, and Bucana C.** Blood levels of alpha-tocopherol in a disorder of lipid peroxidation: Batten's disease. *Am J Clin Nutr* 27: 1152–1157, 1974.
34. **Vance JE, Stone SJ, and Faust JR.** Abnormalities in mitochondria-associated membranes and phospholipid biosynthetic enzymes in the mnd/mnd mouse model of neuronal ceroid lipofuscinosis. *Biochim Biophys Acta* 1344: 286–299, 1997.
35. **Vesa J, Chin MH, Oelegeschlager K, Isosomppi J, Dell-Angelica EC, Jalanko A, and Peltonen L.** Neuronal ceroid lipofuscinoses are connected at molecular level: interaction of CLN5 protein with CLN2 and CLN3. *Mol Biol Cell* 13: 2410–2420, 2002.
36. **Weimer JM, Kriscenski-Perry E, Elshatory Y, and Pearce DA.** The neuronal ceroid lipofuscinoses: mutations in different proteins result in similar disease. *Neuromolec Med* 1: 111–124, 2002.
37. **Wheeler RB, Sharp JD, Mitchell WA, and Bate SL.** A new locus for variant late infantile neuronal ceroid lipofuscinosis: CLN7. *Mol Genet Metab* 66: 337–338, 1999.
38. **Wolfe LS, Ivy G, and Wiktop CJ.** Dolichols, lysosomal membrane turnover and relationship to the accumulation of ceroid and lipofuscin in inherited diseases, Alzheimer's disease and ageing. *Chem Scr* 27: 79–84, 1987.